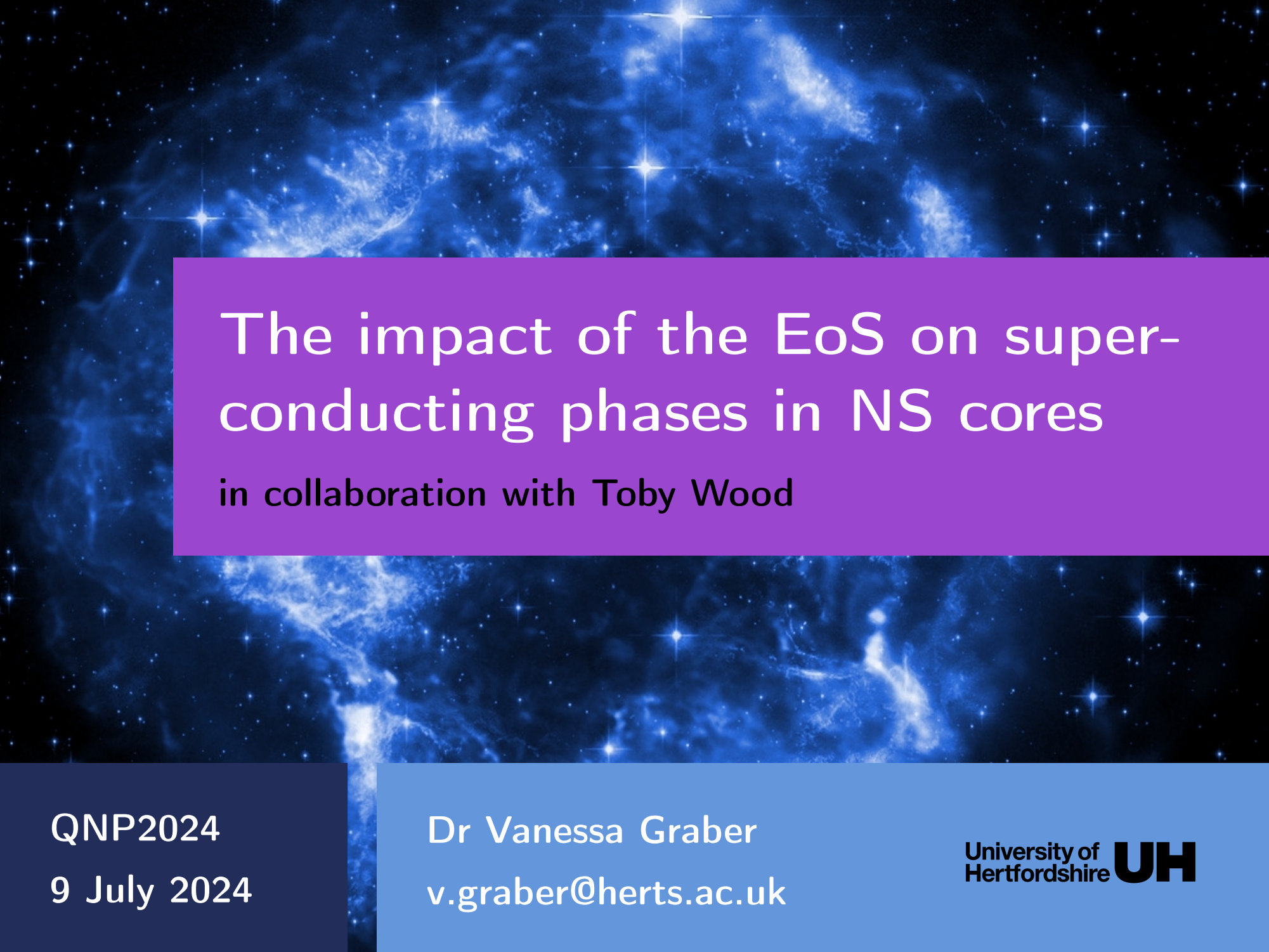

The impact of the EoS on superconducting phases in NS cores

in collaboration with Toby Wood

QNP2024

9 July 2024

Dr Vanessa Graber

v.graber@herts.ac.uk

University of Hertfordshire UH

Motivation

Core magnetic field

- Neutron star **magnetic fields** play a **crucial role** in astrophysics, e.g.:
  - explain the high activity of magnetars & high-B field pulsars.
  - field evolution linked to neutron star ‘metamorphosis‘.
  - influence the dynamics of binary neutron star mergers.
  - related to many astrophysical phenomena (e.g., FRBs, GRBs).
- While a lot of progress has been made in modelling the exterior and crustal magnetic fields, there are still **many open questions** regarding the **field in the core**, carrying a significant fraction of the magnetic energy.
- **Open problems concern**, e.g., *correct* multi-fluid description of matter, ambipolar diffusion, role of crust-core interface, evolution time-scales for type-II superconducting matter, and possibility of *fast* core dissipation.

Motivation

Superconductivity

- The conditions in the interior are such that nucleons can undergo **phase transitions** into **superfluid states** as a result of Cooper pairing. Detailed gap calculations suggest the following **core critical temperatures**:

$$T_{\mathrm{c,\,protons}} \sim 10^9 - 10^{10}\,\mathrm{K}, \qquad T_{\mathrm{c,\,neutrons}} \sim 10^8 - 10^9\,\mathrm{K}, \tag{1}$$

- Our understanding of NS superconductivity is mainly based on **time-independent, single-component** considerations (Baym, Pethick & Pines, 1969):
  - Outer-core protons are in a type-II state with flux confined to a fluxtube array.
  - In the inner core, a transition to an intermediate type-I state takes place.
  - Magnetic flux expulsion times are very long, leading to a meta-stable state.

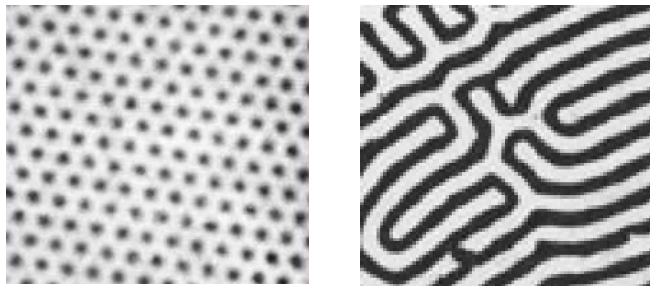

Figure 1: Laboratory type-II and intermediate type-I superconductor (Brandt & Essmann, 1987).

Approach

Condensate coupling

What happens to this picture of core superconductivity when coupling (specifically entrainment) between the condensates is included?

- Expanding **earlier works** (Alpar, Langer & Sauls, 1984; Charbonneau & Zhitnitsky, 2007; Alford & Good, 2008; Haber & Schmitt, 2017), we use techniques for laboratory systems to construct **phase diagrams** by deducing the protons' ground state in presence of a magnetic field (Wood & Graber, 2022).

- With entrainment, **velocity-dependent terms** in energy density read

$$F_{\mathsf{vel}} = \tfrac{1}{2} m n_{\mathrm{p}} |\mathsf{V}_{\mathrm{p}}|^2 + \tfrac{1}{2} m n_{\mathrm{n}} |\mathsf{V}_{\mathrm{n}}|^2 - \tfrac{1}{2} \rho^{\mathrm{pn}} |\mathsf{V}_{\mathrm{p}} - \mathsf{V}_{\mathrm{n}}|^2 , \tag{2}$$

where $n_{\mathrm{p,n}}$ are the nucleon number densities, the coefficient $\rho^{\mathrm{pn}} < 0$ determines the strength of entrainment (Andreev & Bashkin, 1976) and $\mathsf{V}_{\mathrm{p,n}}$ are superfluid velocities related to canonical momenta, i.e., $\propto \nabla \arg \psi_{\mathrm{x}}$.

Ginzburg–Landau model

- In a **mean-field framework**, entrainment first enters at 4th order in $\psi_{\mathrm{n,p}}$ and 2nd order in their derivatives, i.e., we require a linear combination of terms $|\psi_x|^2|\boldsymbol{\nabla}\psi_y|^2, \psi_x\psi_y\boldsymbol{\nabla}\psi_x^\star\cdot\boldsymbol{\nabla}\psi_y^\star, \psi_x\psi_y^\star\boldsymbol{\nabla}\psi_x^\star\cdot\boldsymbol{\nabla}\psi_y, \psi_x^\star\psi_y^\star\boldsymbol{\nabla}\psi_x\cdot\boldsymbol{\nabla}\psi_y$ where $x, y \in \{\mathrm{p}, \mathrm{n}\}$. **Galilean invariance** can be used to simplify the sum.

- The total **free energy density** of our two-component superconductor is

$$
\begin{aligned}
F[\psi_\mathsf{p}, \psi_\mathsf{n}, \mathsf{A}] = {} & \tfrac{1}{8\pi}|\boldsymbol{\nabla}\times\mathsf{A}|^2 + \tfrac{g_{\mathsf{pp}}}{2}\left(|\psi_\mathsf{p}|^2 - \tfrac{n_\mathsf{p}}{2}\right)^2 + \tfrac{g_{\mathsf{nn}}}{2}\left(|\psi_\mathsf{n}|^2 - \tfrac{n_\mathsf{n}}{2}\right)^2 \\
& + g_{\mathsf{pn}}\left(|\psi_\mathsf{p}|^2 - \frac{n_\mathsf{p}}{2}\right)\left(|\psi_\mathsf{n}|^2 - \tfrac{n_\mathsf{n}}{2}\right) + \tfrac{\hbar^2}{4m_\mathsf{u}}\left|\left(\boldsymbol{\nabla} - \tfrac{2\mathrm{i}e}{\hbar c}\mathsf{A}\right)\psi_\mathsf{p}\right|^2 + \tfrac{\hbar^2}{4m_\mathsf{u}}|\boldsymbol{\nabla}\psi_\mathsf{n}|^2 \\
& + h_1\left|\left(\boldsymbol{\nabla} - \tfrac{2\mathrm{i}e}{\hbar c}\mathsf{A}\right)(\psi_\mathsf{n}^\star\psi_\mathsf{p})\right|^2 + \tfrac{h_2 - h_1}{2}\boldsymbol{\nabla}(|\psi_\mathsf{p}|^2)\cdot\boldsymbol{\nabla}(|\psi_\mathsf{n}|^2) \\
& + \tfrac{h_3}{4}\left(\left|\boldsymbol{\nabla}(|\psi_\mathsf{p}|^2)\right|^2 + \left|\boldsymbol{\nabla}(|\psi_\mathsf{n}|^2)\right|^2\right), \qquad (3)
\end{aligned}
$$

where $g_{\mathrm{pp,nn}}$ define the self-repulsion of the condensates, $g_{\mathrm{pn}} \approx 0$ their mutual repulsion and h_i are related to the condensates' coupling.

Approach

Two thought experiments

- To find the **ground state** in the presence of an **imposed magnetic field**, we can control (i) the thermodynamic external magnetic field H, or (ii) the magnetic flux density, $\mathrm{B} = \boldsymbol{\nabla} \times \mathrm{A}$, by imposing a mean flux $\overline{B}$.

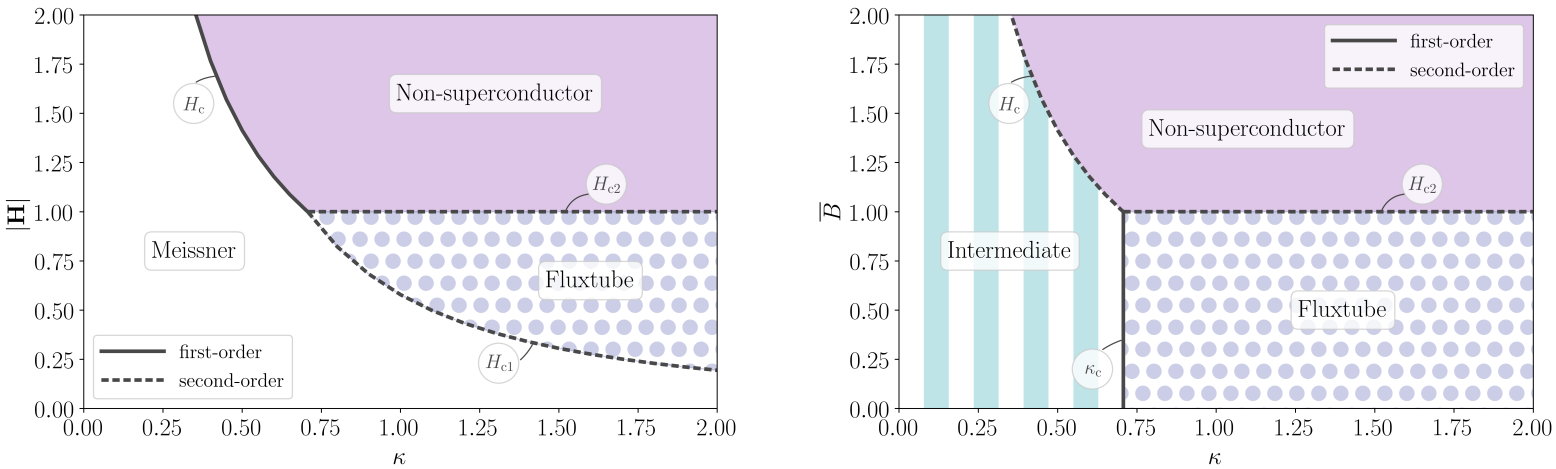

Figure 2: Phase diagrams for a one-component superconductor, for different values of the GL parameter, κ.

Case (ii) approximates the **neutron star interior**, which becomes superconducting as the star cools in the presence of pre-existing flux.

Phase diagrams

- For two-component systems, phase diagrams look more complicated and we obtain additional **mixed states** as a result of condensate interactions. These are marked by **first-order transitions** at $H_{c1'} < H_{c1}$ and $H_{c2'} > H_{c2}$.

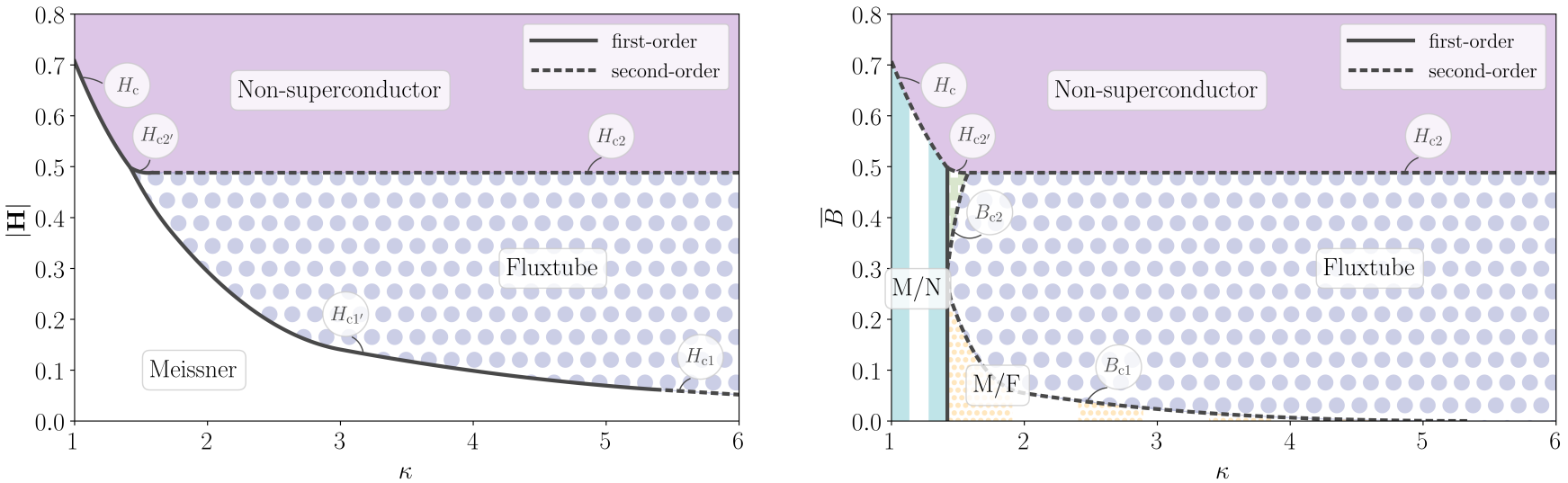

Figure 3: Phase diagrams for our two-component superconductor as a function of κ, and $\sqrt{g_{\mathbf{nn}} n_{\mathbf{n}} / g_{\mathbf{pp}} n_{\mathbf{p}}} = 0.371$, $n_{\mathbf{p}}/n_{\mathbf{n}} = 0.097$, $g_{\mathrm{np}} = 0$, $h_{\mathbf{1}} = 0.102$, $h_{\mathbf{2}} = 0.387$, and $h_{\mathbf{3}} = 0.263$. The shading is indicative of the actual distribution of magnetic flux.

Results

Mixed states

- We find inhomogeneous regimes where fluxtube and non-superconducting regions (left) as well as Meissner and fluxtube regions (right) alternate.

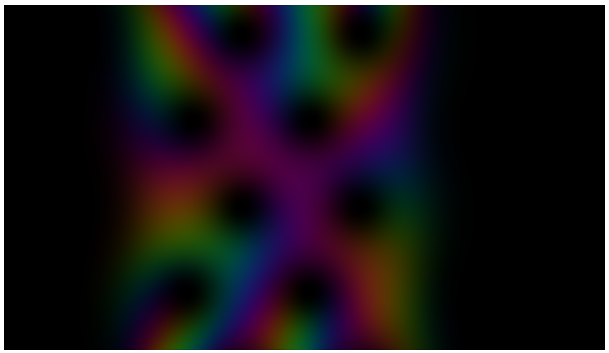

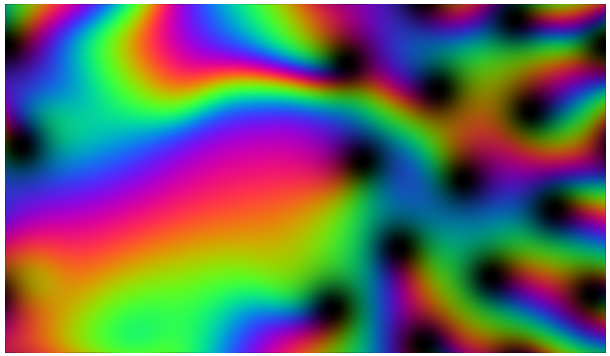

Figure 4: Inhomogeneous ground states, where brightness and hue indicate the density and phase of the proton order parameter, $\psi_{\mathbf{p}}$, respectively.

- Reminiscent of **type-1.5 superconductivity** in terrestrial systems $\Rightarrow$ entrainment causes fluxtube repulsion on short scales & attraction on large scales, resulting in mixed states.

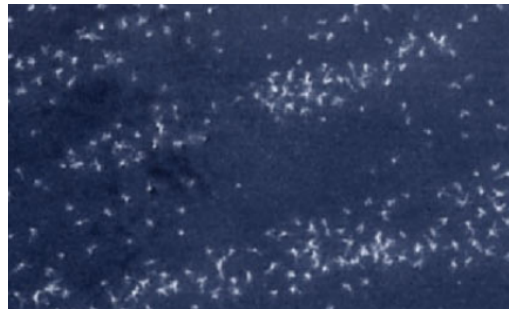

Figure 5: Image of multi-band SC Mg_2B (Moshchalkov et al., 2009).

Results

Skyrme connection

- After determining the **composition** based on the **full Skyrme model**, we link our Ginzburg–Landau model to a reduced Skyrme functional to obtain the coefficients h_i and determine the ground state at different densities.
- To determine g_{pp} and g_{nn}, we consider the CCDK (protons) and TToa (neutrons) gaps motivated by Cas A cooling observations (Ho et al., 2015).

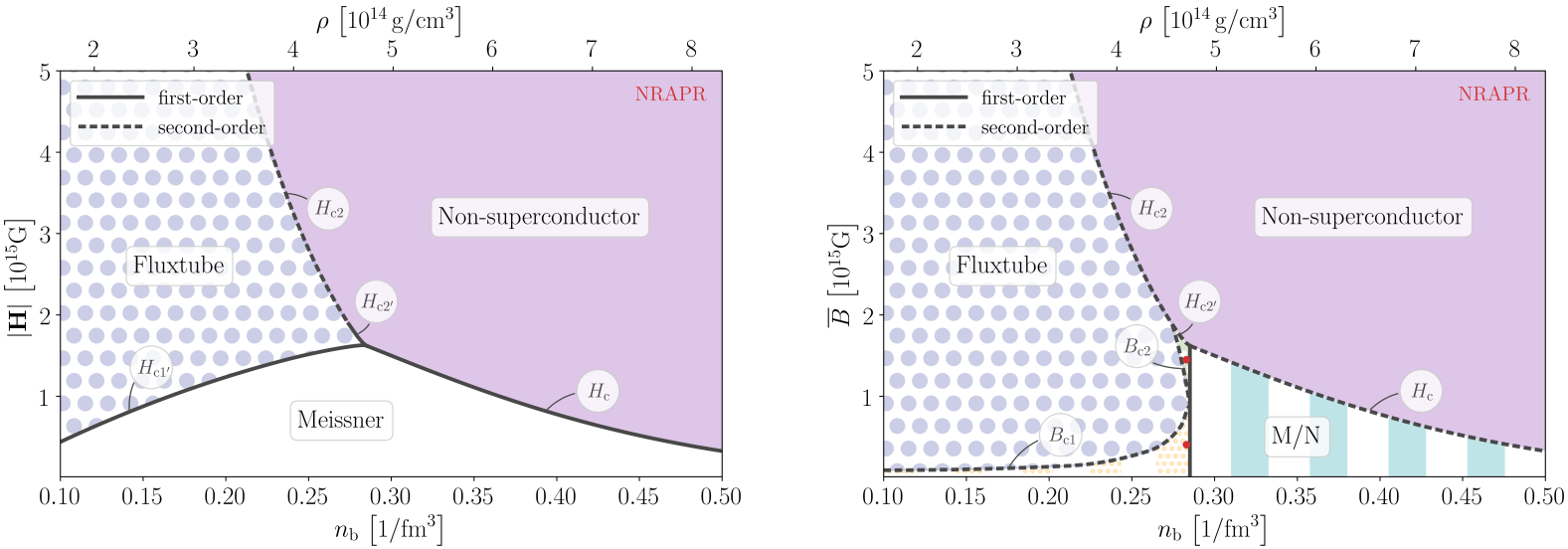

Figure 6: Phase diagrams for the NRAPR equation of state as a function of density.

Results

Different EoSs

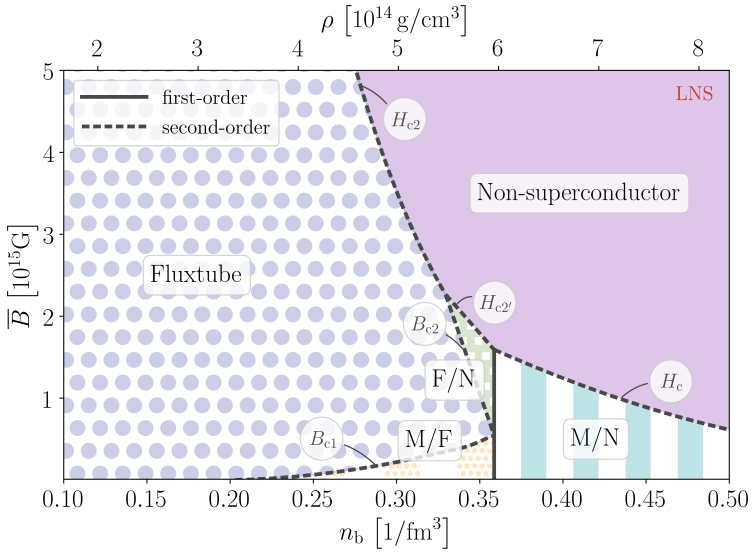

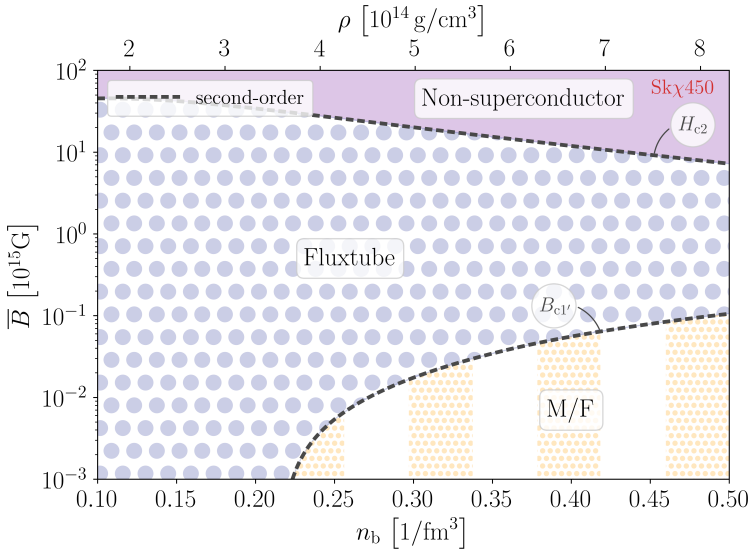

We find mixed states for all six Skyrme functionals but their locations and extents vary significantly between different EoS models!

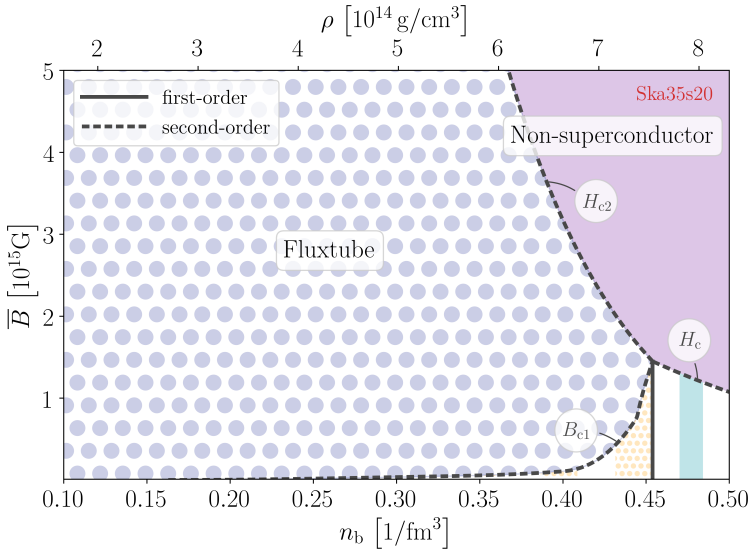

THANK YOU!

Appendix

Two core condensates

- Detailed BCS calculations provide **pairing energy gaps** Δ, associated with the **critical temperatures** T_c for the superfluid and superconducting phase transitions. Two models supported by observed cooling of CasA:

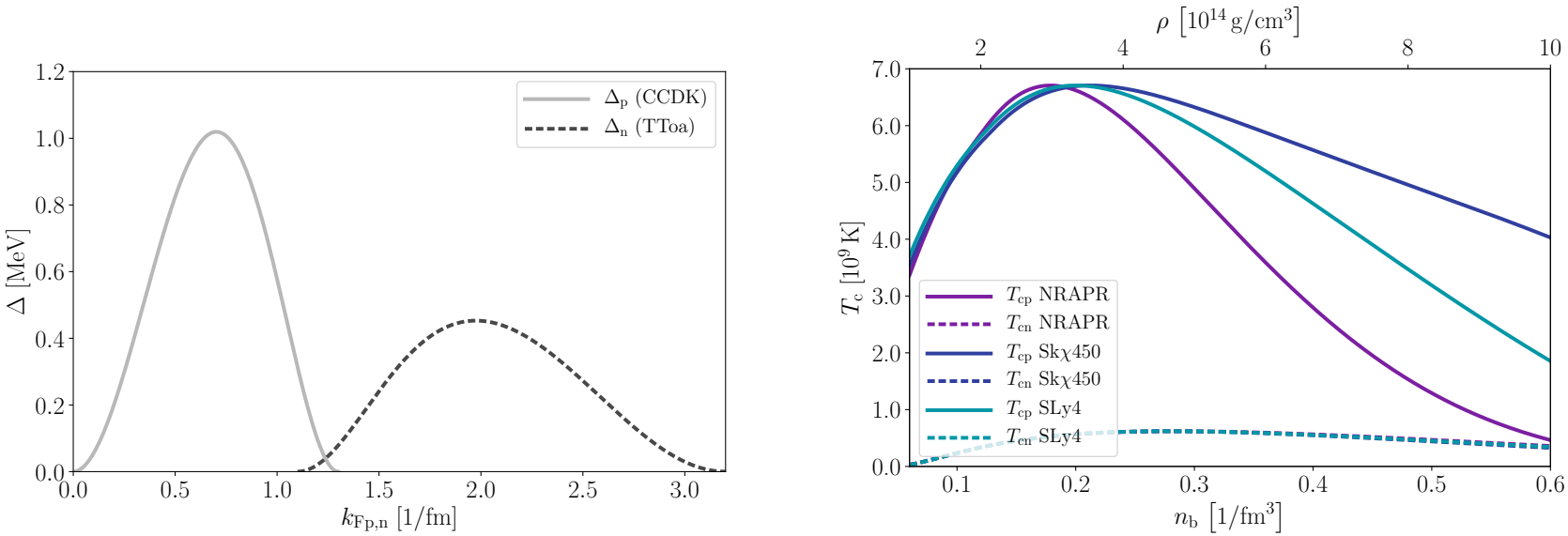

Figure 7: Left: Parametrised proton (singlet) and neutron (triplet) gaps as a function of Fermi wave numbers (Ho et al., 2015). Right: Critical temperatures of core superconductivity/superfluidity as a function of the number and mass density. The curves are computed for three Skyrme equations of state (Chamel, 2008).

Appendix

The (old) type-II picture

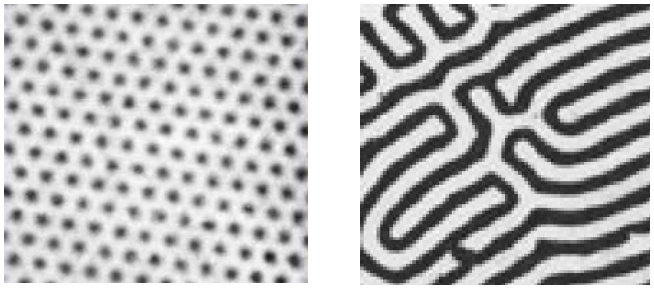

Figure 8: Type-II and intermediate type-I state (Brandt & Essmann, 1987).

- Due to high conductivity, the magnetic flux cannot be expelled from their interiors $\Rightarrow$ neutron stars do not exhibit Meissner effect and are in a **metastable** state (Baym, Pethick & Pines, 1969; Ho, Andersson & Graber, 2017).

- State depends on **characteristic lengthscales** and standard considerations give $\kappa = \lambda_\star/\xi_{\rm ft} > 1/\sqrt{2}$ in the outer core, i.e., a **type-II state** with

$$H_{\rm c1} = 4\pi\mathcal{E}_{\rm ft}/\phi_0 \sim 10^{14}\,{\rm G}, \qquad H_{\rm c2} = \phi_0/(2\pi\xi_{\rm ft}^2) \sim 10^{15}\,{\rm G}. \tag{4}$$

- Each fluxtube carries a **flux quantum** $\phi_0 = hc/2e \approx 2.1\times10^{-7}\,{\rm G\,cm^2}$. All flux quanta add up to the total magnetic flux, so that the **averaged magnetic induction** is related to the fluxtube area density $\mathcal{N}_{\rm ft}$:

$$B = \mathcal{N}_{\rm ft}\phi_0, \quad \rightarrow \quad \mathcal{N}_{\rm ft} \approx 4.8\times10^{18}\,\left(B/10^{12}\,{\rm G}\right)\,{\rm cm^{-2}}. \tag{5}$$

Appendix

Skyrme connection

- We connect energy functional to the **Skyrme interaction** to obtain coefficients h_i that allow a **realistic description** of the neutron star interior:

$$h_1 = C_0^\tau - C_1^\tau\,, \qquad h_2 = -4C_0^{\Delta\rho} + 4C_1^{\Delta\rho}\,, \tag{6}$$

$$h_3 = h_4 = C_0^\tau + C_1^\tau - 4C_0^{\Delta\rho} - 4C_1^{\Delta\rho}\,. \tag{7}$$

- The parameter h_1 controls the entrainment (Chamel & Haensel, 2006)

$$\rho^{\mathrm{pn}} = -\frac{2}{\hbar^2} h_1 \rho_{\mathrm{n}} \rho_{\mathrm{p}}. \tag{8}$$

- We also use the Skyrme model to determine the **stellar composition** (solving for baryon conservation, charge neutrality, beta equilibrium and muon production rate) (Chamel, 2008), but a separate **parametrisation** for the **SF/SC gaps** (Andersson, Comer & Glampedakis, 2005; Ho et al., 2015).

Appendix

Thought experiments

- To find the **ground state** for our system in the presence of an **imposed magnetic field**, we can perform two distinct experiments: we control (i) the magnetic flux density, $\mathrm{B} = \boldsymbol{\nabla} \times \mathrm{A}$, by imposing a mean or net magnetic flux, or (ii) the thermodynamic external magnetic field, H.

- In the first case, we minimise the **Helmholtz free energy**, $\mathcal{F} = \langle F \rangle$, where the angled brackets represent some kind of integral over our physical domain $\Rightarrow$ closely approximates the conditions in the neutron star core, which becomes superconducting as the star cools in the presence of pre-existing magnetic field. The ground state can be **inhomogeneous**.

- In the second case, we minimise the dimensionless **Gibbs free energy**, $\mathcal{G} = \mathcal{F} - 2\kappa^2 \mathrm{H} \cdot \langle \mathrm{B} \rangle$. In an unbounded domain, the ground state is guaranteed to be **homogeneous**, and the phase diagram simpler.

Appendix

Euler-Lagrange equations

- Whether we work with $\mathcal{F}$ or $\mathcal{G}$, we obtain the same equations of motion:

$$\kappa^2 \boldsymbol{\nabla} \times (\boldsymbol{\nabla} \times \mathrm{A}) = \Im \left\{ \psi_\mathrm{p}^\star (\boldsymbol{\nabla} - \mathrm{iA}) \psi_\mathrm{p} + \frac{h_1}{\epsilon} \psi_\mathrm{n} \psi_\mathrm{p}^\star (\boldsymbol{\nabla} - \mathrm{iA})(\psi_\mathrm{n}^\star \psi_\mathrm{p}) \right\} , \tag{9}$$

$$\begin{aligned} \nabla^2 \psi_\mathrm{n} = {} & R^2 (|\psi_\mathrm{n}|^2 - 1)\psi_\mathrm{n} + \alpha (|\psi_\mathrm{p}|^2 - 1)\psi_\mathrm{n} \\ & - h_1 \psi_\mathrm{p} (\boldsymbol{\nabla} + \mathrm{iA})^2 (\psi_\mathrm{p}^\star \psi_\mathrm{n}) \\ & - \psi_\mathrm{n} \nabla^2 \left(\frac{h_2 - h_1}{2} |\psi_\mathrm{p}|^2 + \frac{h_3}{2\epsilon} |\psi_\mathrm{n}|^2 \right) , \end{aligned} \tag{10}$$

$$\begin{aligned} (\boldsymbol{\nabla} - \mathrm{iA})^2 \psi_\mathrm{p} = {} & (|\psi_\mathrm{p}|^2 - 1)\psi_\mathrm{p} + \frac{\alpha}{\epsilon} (|\psi_\mathrm{n}|^2 - 1)\psi_\mathrm{p} \\ & - \frac{h_1}{\epsilon} \psi_\mathrm{n} (\boldsymbol{\nabla} - \mathrm{iA})^2 (\psi_\mathrm{n}^\star \psi_\mathrm{p}) \\ & - \psi_\mathrm{p} \nabla^2 \left(\frac{h_2 - h_1}{2\epsilon} |\psi_\mathrm{n}|^2 + \frac{h_3}{2} |\psi_\mathrm{p}|^2 \right) . \end{aligned} \tag{11}$$

Appendix

Energy minimisation

- F is approximated numerically on a regular 2D grid. The order parameters ψ_p and ψ_n are defined on the gridpoints as $\psi_\mathrm{p}^{i,j}$ and $\psi_\mathrm{n}^{i,j}$, while the vector field A has two components, (A_x, A_y), defined on the corresponding links between the gridpoints, i.e., we have $A_x^{i+1/2,j}$ and $A_y^{i,j+1/2}$.

- The gauge coupling between ψ_p and A is implemented using a **Peierls substitution** to preserve (discrete) gauge symmetry, e.g.,

$$\left|\left(\frac{\partial}{\partial x} - \mathrm{i}A_x\right)\psi_\mathrm{p}\right| = \left|\frac{\partial}{\partial x}\exp(-\int \mathrm{i}A_x\,\mathrm{d}x)\psi_\mathrm{p}\right|$$

$$\Rightarrow \left|\left(\frac{\partial}{\partial x} - \mathrm{i}A_x\right)\psi_\mathrm{p}\right|^{i+1/2,j} \simeq \frac{1}{\delta x}\left|\exp(-\mathrm{i}A_x^{i+1/2,j}\,\delta x)\psi_\mathrm{p}^{i+1,j} - \psi_\mathrm{p}^{i,j}\right|. \qquad (12)$$

- This leads to a discrete approximation $\mathcal{F}_\mathsf{dis}[\psi_\mathrm{p}^{i,j}, \psi_\mathrm{n}^{i,j}, A_x^{i+1/2,j}, A_y^{i,j+1/2}]$ and we obtain the ground state using a gradient-descent, iteration method.

Appendix

Energy per flux quantum

- We solve the Euler-Lagrange equations with **quasi-periodic boundary conditions** (Wood et al., 2019), which involves specifying the domain size $L_x \times L_y$, and the number N of magnetic flux quanta within the domain
  $\Rightarrow$ different choices allow comparing **square** and **hexagonal lattices**.

- The Helmholtz free energy per magnetic flux quantum per unit length is

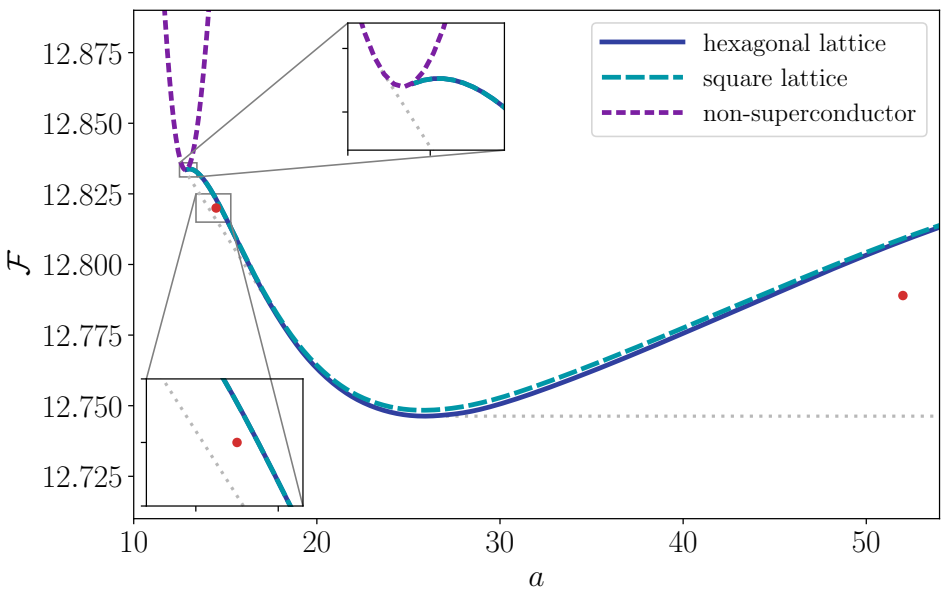

$$\mathcal{F} \equiv \frac{1}{N} \int_{x=0}^{L_x} \int_{y=0}^{L_y} F \, \mathrm{d}x \, \mathrm{d}y \, . \tag{13}$$

Figure 9: Helmholtz free energy per flux quantum per unit length, $\mathcal{F}$, as a function of the area per magnetic flux quantum, $a = 2\pi/\overline{B}$, for the NRAPR EoS at $n_\mathrm{b} = 0.2831/\mathrm{fm}^3$. The energy in the square (long-dashed, cyan) and hexagonal (solid, blue) lattice states matches smoothly onto the energy of the non-superconducting state (short-dashed, purple) at $a \simeq 12.9$.

Appendix

(A few) caveats

- We assume that the **Skyrme model** correctly describes interactions up to the neutron star centre. If exotic particles / non-nucleonic matter are present, this would modify the picture at high densities.
- Our **superfluid gap models** (p: CCDK, n: TToa) are motivated by cooling observations of the Cas A supernova remnant but inconsistent with the mean-field description of the interacting particles.
- Our Ginzburg–Landau model is **time-independent** and neglects **rotation**, i.e., we do not capture dynamics or incorporate neutron vortices *yet*, which are crucial to get the full macroscopic picture.
- For a full dynamical model, we would need to incorporate the **normal electron component**. We do not have the formalism to consistently include such a (particle) component in the Ginzburg–Landau model *yet*.

Appendix

References I

Alford M. G., Good G., 2008, Physical Review B, 78, 024510

Alpar M. A., Langer S. A., Sauls J. A., 1984, The Astrophysical Journal, 282, 533

Andersson N., Comer G., Glampedakis K., 2005, Nuclear Physics A, 763, 212

Andreev A. F., Bashkin E. P., 1976, Soviet Physics JETP, 42, 164

Baym G., Pethick C. J., Pines D., 1969, Nature, 224, 673

Chamel N., 2008, Monthly Notices of the Royal Astronomical Society, 388, 737

Chamel N., Haensel P., 2006, Physical Review C, 73, 045802

Charbonneau J., Zhitnitsky A. R., 2007, Physical Review C, 76, 015801

Haber A., Schmitt A., 2017, Physical Review D, 95, 116016

Ho W. C. G., 2015, Monthly Notices of the Royal Astronomical Society, 452, 845

Ho W. C. G., Elshamouty K. G., Heinke C. O., Potekhin A. Y., 2015, Physical Review C, 91, 015806

Ho W. W. C. G., Andersson N., Graber V., 2017, Physical Review C, 96, 065801

Moshchalkov V. V. et al., 2009, Physical Review Letters, 102, 117001

Wood T. S., Graber V., 2022, Universe, 8, 228

Wood T. S., Mesgarnezhad M., Stagg G. W., Barenghi C. F., 2019, Physical Review B, 100, 024505